

RESEARCH ARTICLE

*Role of Leukocytes in Cardiovascular Disease*

**Mast cells in failing human hearts demonstrate transcriptomic activation of pathways involved in cardiac remodeling**

 Mikael Sandstedt,<sup>1,2</sup> Markus Johansson,<sup>3</sup> Marianne Jonsson,<sup>1,2</sup>  Kristina Vukusic,<sup>1</sup>  Benjamin Ulfenborg,<sup>3</sup> Maria Sandstedt,<sup>1,4,5</sup>  Lillemor Mattsson Hultén,<sup>2,5</sup>  Victoria Rotter Sopasakis,<sup>1,2</sup> Göran Dellgren,<sup>5,6</sup>  Anders Jeppsson,<sup>5,7</sup>  Jane Synnergren,<sup>3,5</sup> and  Joakim Sandstedt<sup>1,2</sup>

<sup>1</sup>Department of Laboratory Medicine, Institute of Biomedicine, Sahlgrenska Academy, University of Gothenburg, Gothenburg, Sweden; <sup>2</sup>Region Västra Götaland, Department of Clinical Chemistry, Sahlgrenska University Hospital, Gothenburg, Sweden; <sup>3</sup>Department of Biology and Bioinformatics, School of Bioscience, University of Skövde, Skövde, Sweden; <sup>4</sup>Region Västra Götaland, Children's Heart Center, The Queen Silvia Children's Hospital, Sahlgrenska University Hospital, Gothenburg, Sweden; <sup>5</sup>Department of Molecular and Clinical Medicine, Institute of Medicine, Sahlgrenska Academy, University of Gothenburg, Gothenburg, Sweden; <sup>6</sup>Department of Surgery, Institute of Clinical Sciences, Sahlgrenska Academy, University of Gothenburg, Gothenburg, Sweden; and <sup>7</sup>Region Västra Götaland, Department of Cardiothoracic Surgery, Sahlgrenska University Hospital, University of Gothenburg, Gothenburg, Sweden

**Abstract**

Intracardiac mast cells (CMCs) have previously been shown to contribute to adverse remodeling and heart failure in animal models. As CMCs in human hearts remain unexplored, the aim of this study was to investigate the pathophysiological relevance of human CMCs through transcriptomic profiling. Biopsies were collected from the four heart chambers of heart failure patients undergoing heart transplantation surgery ( $n = 9$ ), as well as from deceased organ donors without chronic heart failure ( $n = 5$ ). Using flow cytometry, C-kit<sup>+</sup>CD45<sup>+</sup> CMCs and C-kit<sup>-</sup>CD45<sup>+</sup> hematopoietic cells were identified in all failing and nonfailing hearts and were sorted for RNA sequencing analysis. In comparison with other hematopoietic C-kit<sup>-</sup>CD45<sup>+</sup> cells and CMCs in nonfailing hearts, CMCs in failing hearts demonstrated significant activation of pathways involved in cardiac remodeling and heart failure, including fibrosis-associated and inflammatory pathways. Our results support a role for mast cells in human heart failure and constitute the first in-depth characterization of mast cells in the nonfailing and failing human heart.

**NEW & NOTEWORTHY** Intracardiac mast cells (CMCs) have been shown to contribute to remodeling and fibrosis in animal models. No phenotypical characterization of human CMCs has been conducted before the current transcriptomic profiling study. CMCs isolated from failing human hearts demonstrated activated pathways involved in cardiac remodeling and fibrosis, both compared with other hematopoietic cells and to CMCs in nonfailing hearts. The study suggests that CMCs may constitute a novel candidate for modulation in human heart failure.

*heart failure; immune system; mast cells; normal heart; transcriptomics*

**INTRODUCTION**

Heart failure constitutes a clinical syndrome associated with substantial morbidity and mortality (1). Although treatment and diagnosis of heart failure have improved, prognosis remains poor. Multiple etiologies, including myocardial ischemia, myocarditis, valvular disease, and hypertension, may all result in heart failure (2). Immune system-associated mechanisms have been reported to contribute to cardiac remodeling in numerous settings. Mast cells constitute cells of the innate immune system which upon activation may

secrete signaling factors such as histamine, cytokines, growth factors, prostaglandins and leukotrienes, as well as the proteases tryptase and chymase (3). The pathophysiological relevance of mast cells in cardiovascular disease has been established during the past decades.

The existence of tissue-resident intracardiac mast cells (CMCs) has been reported in multiple species, including mice (4), rats (5, 6), and humans (7). Most cardiac diseases result in increased CMC density and activity in the acute and/or chronic setting, as demonstrated through animal models of pressure/volume overload (5, 8), autoimmune/



Correspondence: M. Sandstedt (mikael.sandstedt@gu.se).  
Submitted 25 November 2025 / Revised 16 December 2025 / Accepted 6 March 2026



viral myocarditis (9, 10), and myocardial infarction (MI) (11, 12). In spontaneously hypertensive rats, CMCs may contribute to fibrosis via secretion of cytokines, growth factors, as well as the mast cell-associated proteases tryptase and chymase (5, 13). Mast cell-associated signaling may also contribute to cardiac hypertrophy, fibrosis, and dysfunction following autoimmune myocarditis (9, 14). Similarly, CMCs have been shown to contribute to cardiac inflammation, fibrosis, and dysfunction secondary to viral myocarditis (10). Finally, contrasting effects of CMCs and mast cell-associated factors have been proposed following MI, including both stimulating and inhibiting effects on cardiac fibrosis (15).

Patients with chronic heart failure have demonstrated an accumulation of CMCs in previous studies (16, 17). The concentration of CMCs has been shown to be similarly elevated in the ventricles of ischemic and nonischemic failing human hearts in comparison with nonfailing control hearts (16). Human CMCs have been shown to express the pan-hematopoietic marker CD45, and most cells express the hematopoietic stem cell/mast cell marker C-kit/CD117 as well as tryptase and chymase (7). The amount of cardiac fibrosis (17, 18) has been shown to be positively correlated with the CMC density in human hearts.

As most studies of human and nonhuman CMCs have been limited to in situ histological/immunohistochemical analyses or analyses on tissue-level, no extensive phenotypic characterization of CMCs has previously been conducted. Whether the transcriptome of human CMCs may differ between failing and nonfailing hearts is, therefore, not known. Possible transcriptomic differences between human CMCs and other hematopoietic cells, as well as for CMCs in the different chambers of the human heart, have also not been explored. Thus, in the current study, C-kit<sup>+</sup>CD45<sup>+</sup> mast cells and C-kit<sup>-</sup>CD45<sup>+</sup> hematopoietic cells in failing and nonfailing human hearts were analyzed using flow cytometry (FACS) and sorted for RNA sequencing analysis. The transcriptomic analysis of CMCs in failing hearts revealed significant activation of pathways involved in cardiac remodeling and heart failure. Our findings, therefore, support a pathophysiological role for CMCs in human heart failure and that CMCs could constitute a novel candidate for intervention.

## MATERIALS AND METHODS

### Study Participants

The study was conducted after approval of the local ethics committee at the University of Gothenburg (Nos. 436-15 and 596-11) and in accordance with the Helsinki Declaration as revised 2013. Following explantation of the heart during heart transplantation, biopsies were collected from the four chambers of terminal heart failure patients at Sahlgrenska University Hospital ( $n = 9$ , Supplemental Table S1). Written informed consent had been obtained. Biopsies were similarly collected from organ donors not suffering from chronic heart failure based on information from medical records and relatives ( $n = 5$ , Supplemental Table S2). The hearts of the included organ donors were ineligible for transplantation, in general due to old age and/or comorbidities. For one donor ("Donor 5," Supplemental Table S2) the heart could not

undergo transplantation as no suitable recipient was available. All donors had documentation of consent for use of organs for transplantation as well as other medical purposes, including research. Due to limited supply of biopsies, material from some of the patients and donors has also been included in other published and unpublished studies (19–23).

### Cell Isolation and Staining

Tissue procurement, cell isolation, staining and flow cytometric analysis, and sorting were conducted as previously described (21). The time span between heart excision and biopsy collection was kept at a minimum while allowing for surgical handling, transportation, and practical preparations. Following excision, hearts were preserved at 4°C. All biopsies were collected within 12 h following excision, and most hearts were processed after only a few hours.

Transmural biopsies were excised from the free wall of the right and left atrium, as well as the right and left ventricle near the apex. Areas with apparent fibrosis were omitted. Biopsies were collected and rinsed in cold phosphate-buffered saline (PBS) to remove blood. After biopsy dissection into small pieces using scissors, enzymatic digestion was conducted using Liberase type TM 0.52 U/mL (Roche, Basel, Switzerland) and DNase type I 2,000 U/mL (Roche or Worthington Biochemical Corporation, Lakewood, NJ) in DMEM:F12 (Thermo Fisher Scientific, Waltham, MA) under magnetic stirring. After 4.5 h, cells were incubated with 0.05% Trypsin-EDTA (Thermo Fisher Scientific), followed by sequential filtering down to 100- $\mu$ m pore size to remove larger cells and tissue fragments.

To optimize expression and detection of cell surface markers, cells underwent epitope regeneration through incubation with DMEM:F12 supplemented with 5% fetal bovine serum (FBS, Sigma-Aldrich, St. Louis, MO) and 1 mM EDTA (Sigma-Aldrich) using mild magnetic stirring for 10–12 h. Epitope regeneration was followed by treatment with nonenzymatic cell dissociation solution (Sigma-Aldrich) and erythrocyte lysis buffer, followed by resuspension in FACS staining buffer [PBS supplemented with 5% FBS, 1% BSA (Sigma-Aldrich) and 2 mM EDTA] and filtering down to 40- $\mu$ m pore size to attain a suspension of single cells without mature cardiomyocytes.

### Cell Staining and Fixation

Cells were stained using 7-AAD (Thermo Fisher Scientific) and antibodies (Supplemental Table S3) for identification of dead cells and cell surface markers. Cells were stored in darkness, on ice, in FACS staining buffer until FACS. In some cases, storage was prolonged for several hours until analysis due to practical circumstances. Such cell samples were fixed using formaldehyde following 7-AAD/antibody staining to stop mRNA degradation. This method has been validated (24) and applied (21) in previous studies. To enable statistical correction, both nonfixed and fixed samples were analyzed and sorted during experiments with sufficient biopsy material and minimal delay until analysis/sorting. In cases with compatible antibody/fluorochrome panels, samples were stained with DAPI (Thermo Fisher Scientific) during fixation

to improve FACS cell identification. Nonfixed cells could not be stained with DAPI as they were not permeable.

### FACS Analysis and Sorting

FACS was conducted using a FACSaria II cell sorter (BD, Franklin Lakes, NJ), with lasers and filters enabling analysis of the implemented fluorochromes, and analysis was performed using FACSDiva version 6.1.1 (BD). Forward scatter versus side scatter, as well as DAPI staining, for fixed samples, were used to identify cells (Supplemental Fig. S1). Dead 7-AAD<sup>+</sup> cells were omitted from further analysis and sorting. A CD45<sup>+</sup> gate was applied to attain adequate separation of the CD45<sup>+</sup>/CD45<sup>-</sup> populations. Due to the relative scarcity of C-kit<sup>+</sup> cells, an exclusive C-kit<sup>+</sup> gating strategy was applied, with < 0.01% false-positive cells based on isotype controls (Supplemental Fig. S2). C-kit<sup>+</sup>CD45<sup>+</sup> and C-kit<sup>-</sup>CD45<sup>+</sup> cells were FACS sorted for further RNA sequencing into separate polypropylene tubes containing either RNase-free PBS (Thermo Fisher Scientific) or RLT buffer including DTT (Qiagen, Hilden, Germany) for fixed and nonfixed samples, respectively. Sorted samples were stored at -80°C until RNA extraction.

### RNA Extraction

Different protocols were used to isolate RNA from fixed and nonfixed samples. DNase concentrations were optimized for fixed, as well as nonfixed samples to minimize genomic DNA contamination without affecting RNA yield and quality.

For nonfixed cell samples, RNA isolation was conducted using the miRNeasy Cells Advanced Micro Kit (Qiagen) with minor modifications. Cells were directly sorted into the RLT buffer with DTT during FACS. Twenty-nanogram carrier RNA (Qiagen) was added to increase RNA yield. DNase I (Qiagen) diluted 1:200 was used according to standard RNeasy protocols from Qiagen. The vacuum manifold QIAvac (Qiagen) was used instead of centrifugation to maximize the volume loaded onto the columns for samples with large volumes. Drying of the column and elution was conducted using centrifugation for all samples.

For formaldehyde fixed cell samples, RNA isolation was conducted using the miRNeasy FFPE kit (Qiagen). DNase I was included for the columns at a dilution of 1:80. Twenty-nanogram carrier RNA was added to increase RNA yield. The QIAvac was used except for drying of the membrane, which was conducted using centrifugation for all samples. RNA was eluted in 20 µL RNase-free water.

### Library Preparation and RNA Sequencing

Library preparation, RNA sequencing, and compilation of raw mRNA count data were conducted by TATAA Biocenter (TATAA Biocenter, Gothenburg, Sweden). Extracted RNA was used to prepare a library using the HTG EdgeSeq transcriptome panel (HTG Molecular Diagnostics, Tucson, AZ) according to the recommendations from the manufacturer. This technique implements a target-based PCR step before RNA sequencing, resulting in near-transcriptomic coverage. Samples underwent RNA sequencing using the Illumina NovaSeq 6000 (Illumina, San Diego, CA) with the S2 flow cell configuration. Fastq files were created using

bcl2fastq, and read quality parameters were assessed using FastQC/MultiQC. Raw mRNA count data (<https://doi.org/10.6084/m9.figshare.30666515>) were generated using the HTG EdgeSeq Parser software (HTG Molecular Diagnostics).

### Statistical Analysis of Flow Cytometric Data

For C-kit<sup>+</sup>CD45<sup>+</sup> and C-kit<sup>-</sup>CD45<sup>+</sup> cells, the percentage of cells, which had stained falsely positive based on isotype controls, was subtracted before calculation of statistics. RStudio version 2023.03.1 with R base version 4.2.1 (R Core Team) (25) was used to conduct statistical analyses. When data deviated from the normal distribution, log transformation was conducted. Comparisons between groups were primarily conducted by analysis of variance (ANOVA) followed by Tukey's post hoc test with the R packages lme4, car, and emmeans. In comparisons between heart chambers for which study participant was included as a block variable, a mixed model was fitted using study participant as random factor. For data that did not fulfill criteria of normal distribution and equal variance, a nonparametric test was calculated using the Prentice test as implemented in the R package muStat. This was followed by Wilcoxon signed-rank test for paired data and Wilcoxon rank-sum test for grouped data. Adjustment for multiple testing was conducted using the Hochberg method as implemented in the p.adjust function in R.

### Statistical Analysis of RNA Sequencing Count Data

See Fig. 1 for a summary of the statistical comparisons. RStudio version 2023.03.1 with R base version 4.2.1 (25) was used for all statistical analyses of RNA sequencing data.

A small number of targets used in the HTG EdgeSeq transcriptome panel represented families of genes. For these gene families, the mean count per gene was used, rounded to the closest integer. For a few genes, the gene was represented both as an individual gene and in a family of genes. In these cases, the individual count was used for analysis.

Genes with very few or no counts in most of the samples were excluded from the analysis. For comparisons between populations and between failing/nonfailing hearts, only genes with at least five counts in at least  $n - 5$  samples were included,  $n$  being the sample size of the smallest compared group. Due to the smaller number of samples included in comparisons between heart chambers, a different numerical cutoff was used for inclusion of genes, that is, genes with at least five counts in at least  $n - 2$  samples.

Normalization of raw count data was conducted using functions in DESeq2 and variance-stabilized transformed values were calculated ("blind" option set to false) and used for principal component analysis (PCA). The 5,000 genes with the highest variance in the samples analyzed were selected as input to PCA using the pcaMethods R package. Missing values were managed using the svdImpute method. Kruskal-Wallis  $H$  tests were calculated for each principal component to determine clustering of samples.

Technical parameters with systematic impact on the transcriptomic pattern of the analyzed samples were identified based on PCA of all samples, as well as samples selected for each statistical comparison as outlined in Fig. 1. Systematic clustering was identified based on fixation, low expression

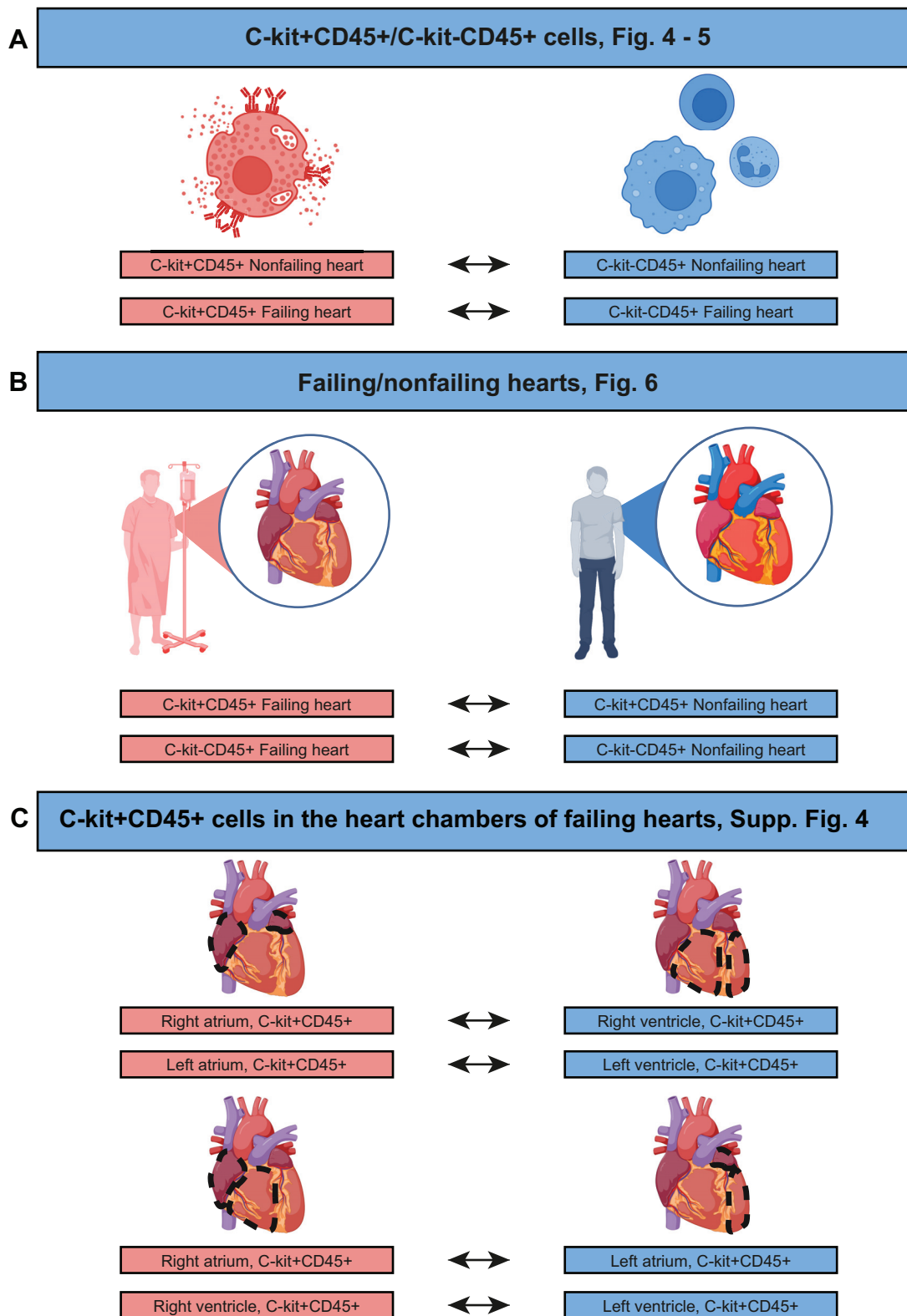


**Figure 1.** Statistical design. Each arrow corresponds to one PCA/IPA analysis. The group constituting the reference level of each IPA analysis has been situated to the right and has been color-coded blue. Three levels of group comparisons were conducted. *A:* C-kit<sup>+</sup>CD45<sup>+</sup> mast cells and C-kit<sup>-</sup>CD45<sup>+</sup> hematopoietic cells were compared in nonfailing and failing hearts, respectively. Samples from all heart chambers were included. C-kit<sup>-</sup>CD45<sup>+</sup> samples constituted reference level. *B:* failing/nonfailing hearts were compared for C-kit<sup>+</sup>CD45<sup>+</sup> and C-kit<sup>-</sup>CD45<sup>+</sup> cells, respectively. Samples from all heart chambers were included. Nonfailing hearts constituted reference level. *C:* C-kit<sup>+</sup>CD45<sup>+</sup> cells isolated from the different heart chambers of failing hearts were compared. Right atrium/right ventricle and left atrium/left ventricle were compared using ventricle as reference level. Right atrium/left atrium and right ventricle/left ventricle were compared using left as reference level. IPA, ingenuity pathway analysis; PCA, principal component analysis. Figure created with a licensed version of BioRender.com.

variability across sequenced targets (“QC2” in the HTG assay) and gDNA contamination (“QC3” in the HTG assay). To minimize the risk of introducing bias through variation in technical parameters, samples that demonstrated low expression variability across sequenced targets were excluded based on the QC2 cutoff recommended by the manufacturer. Furthermore, fixation status and level of gDNA contamination/QC3 were included as correction factors in all subsequent DESeq2 models. Resulting PCA models were assessed to confirm the absence of relevant residual clustering based on fixation status and level of gDNA contamination/QC3.

Based on PCA plots combined with Hotelling’s  $T^2$  statistics, samples that constituted extreme outliers when compared with the majority of samples were identified. A total of 10 outlier samples were identified in the comparisons (Fig. 1) between C-kit<sup>+</sup>CD45<sup>+</sup>/C-kit<sup>-</sup>CD45<sup>+</sup> samples, failing/nonfailing hearts for C-kit<sup>+</sup>CD45<sup>+</sup> samples, and the different heart chambers for C-kit<sup>+</sup>CD45<sup>+</sup> samples. These 10 samples were excluded from all subsequent analyses.

For samples, which constituted technical replicates, that is, two fixed or two nonfixed samples isolated from the same heart chamber of a particular study participant, the “Collapse” function within DESeq2 was used to calculate a mean count matrix for the two samples. For technical replicate pairs in which one sample had been fixed with formaldehyde, whereas the other had not, only the nonfixed sample was included for subsequent analyses.

DESeq2 was used to conduct differential gene expression analysis for the comparisons outlined in Fig. 1. For comparisons between C-kit<sup>+</sup>CD45<sup>+</sup>/C-kit<sup>-</sup>CD45<sup>+</sup> cells as well as between failing/nonfailing hearts, samples from all heart chambers were included as biological replicates. Effect shrinkage was conducted using the lfcShrink function with the adaptive shrinkage estimator from the “ashr” package.

### Ingenuity Pathway Analysis

Canonical pathway analysis was conducted using ingenuity pathway analysis (IPA; QIAGEN Redwood City Inc., Redwood City, CA) based on differentially expressed genes (DEGs) with a log<sub>2</sub> fold change of either ≥1.0 or ≤−1.0. To determine the significance level of enrichment, *P* values were calculated using right-tailed Fisher’s exact tests. The *P* value represents the probability of observing a random overlap between the collection of genes in the input dataset and the genes of a specific IPA pathway. *P* values were adjusted for multiple testing according to the Benjamini–Hochberg procedure. The activation *Z*-score was calculated to estimate the activation state of each pathway. Pathways with *Z*-scores ≥2 and ≤−2 were, respectively, defined as significantly activated and deactivated. Only pathways with an adjusted *P* value < 0.05 and a *Z*-score ≥2, ≤−2 or undetermined (either due to insufficient number of pathway-genes within the dataset or due to the design of the pathway) were reported as significantly enriched. For each group comparison, a selection of the most biologically relevant significant pathways was visualized in a bar plot.

### Cytoscape Analysis

Cytoscape was used to visualize the IPA output to conduct a holistic analysis of the pathway activation patterns. Data

were imported using the EnrichmentMap application. Visualized pathways were limited to significant pathways with adjusted *P* values ≤ 0.05 and *Z*-scores ≥2.0 or ≤−2.0 or undetermined. The nodes of the Cytoscape networks represented individual pathways. Each node was color-coded corresponding to the activated (red, i.e., *Z*-score ≥ 2.0) or deactivated (blue, i.e., *Z*-score ≤ −2.0) status of the pathway. Nodes with undetermined *Z*-scores were color-coded black. The size of each node corresponded to the number of genes constituting the pathway. Overlap between pathways was represented as edges between nodes. The AutoAnnotate function combined with manual curation was used to cluster nodes based on biological relevance. Nodes within each cluster were manually reviewed to identify the dominant enrichment patterns based on the overall activation status of the pathways.

### Upstream Regulator Analysis

IPA was used to predict upstream regulatory elements (UREs) that may explain the observed transcriptomic difference between C-kit<sup>+</sup>CD45<sup>+</sup> samples isolated from nonfailing and failing hearts. All DEGs with an absolute fold change > 2 and a false discovery rate (FDR) value < 0.05 were included, and UREs were limited to genes, RNAs, and proteins.

For each URE, a *Z*-score was calculated based on the known relationship between the DEGs and the URE and the direction of change of the DEGs. Activated and deactivated UREs, respectively, have *Z*-scores >0 and <0. *Z*-scores > 2 or <−2 are considered statistically significant. To identify highly significant UREs, the analysis was limited to UREs with *Z*-scores > 3 or <−3. An overlap *P* value was calculated for each URE using Fisher’s exact test, corresponding to the statistical significance of the overlap between the DEGs and the genes regulated by a URE. Only UREs with an overlap *P* value < 0.01 were analyzed.

Disease and function analysis in IPA was used to identify UREs associated with the terms “Inflammatory response,” “Proliferation of immune cells,” “Leukocyte migration,” “Cell death of immune cells,” “Synthesis of eicosanoid,” “Cardiomyopathy,” “Hypertrophy of cardiac muscle,” “Cell death of cardiomyocytes,” and “Fibrosis of heart.” IPA Knowledge Base was used to identify drugs that interact with the predicted UREs.

## RESULTS

### C-kit<sup>+</sup>CD45<sup>+</sup> Mast Cells Were Identified in All Chambers of Failing and Nonfailing Human Hearts, and Were Significantly Fewer within the Left Ventricle

C-kit<sup>+</sup>CD45<sup>+</sup> cells were identified in all chambers of failing and nonfailing human hearts (Fig. 2, A–C). The portion of C-kit<sup>+</sup>CD45<sup>+</sup> cells was significantly smaller within the left ventricle in comparison with all other heart chambers (Fig. 2C). The portion of C-kit<sup>+</sup>CD45<sup>+</sup> cells did not differ significantly between failing/nonfailing hearts or between ischemic/nonischemic failing hearts. In comparison with C-kit<sup>+</sup>CD45<sup>+</sup> cells, C-kit<sup>-</sup>CD45<sup>+</sup> hematopoietic cells constituted a larger population in all chambers of all analyzed hearts (Fig. 2D).

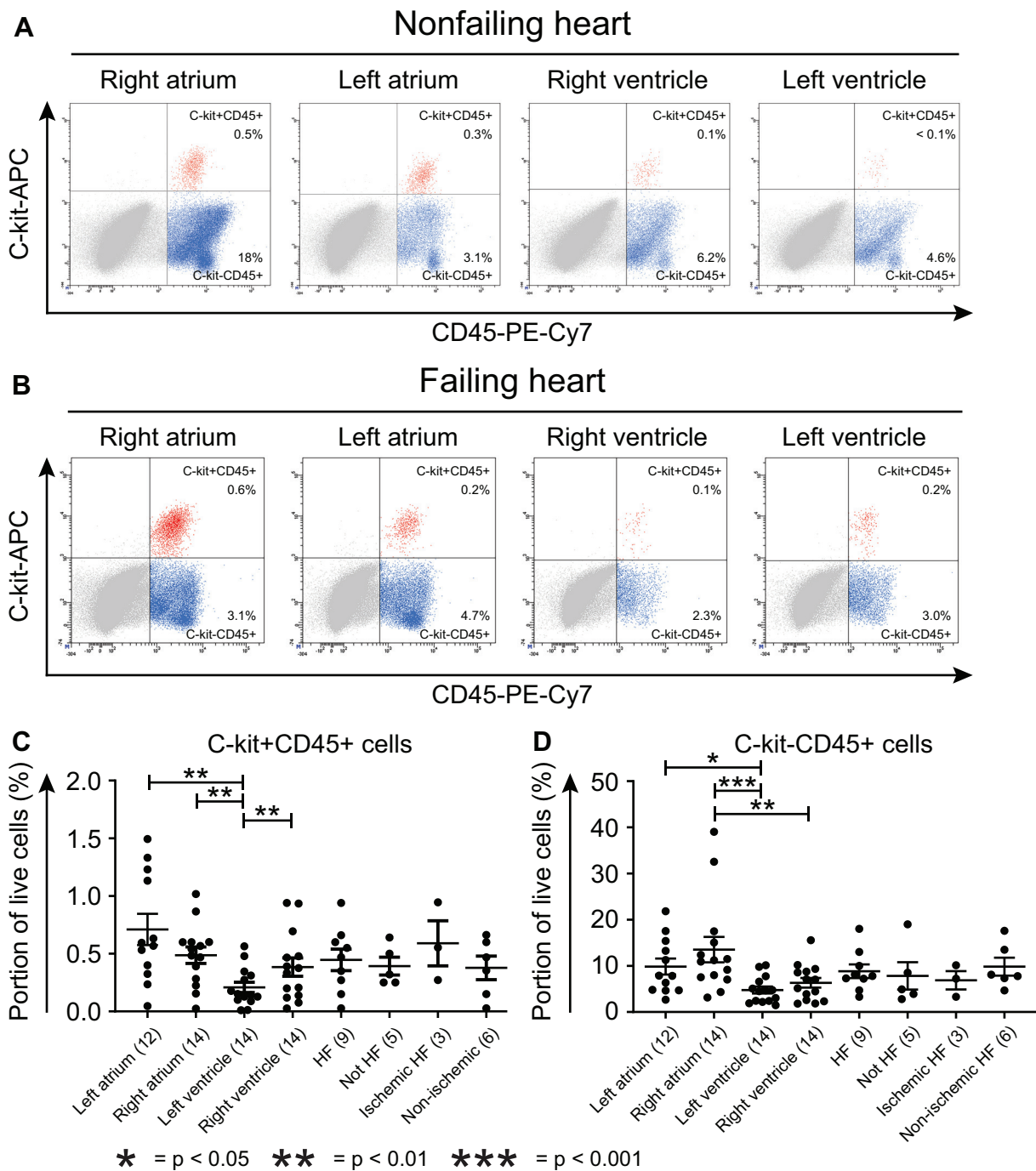


**Figure 2.** Example FACS plots and summary statistics for the different chambers of failing and nonfailing hearts. Scatter plots demonstrating C-kit/CD45 staining for one nonfailing heart (A) and one failing heart (B). Positive staining was determined based on isotype controls (Supplemental Fig. S2). The portions of C-kit<sup>+</sup>CD45<sup>+</sup> and C-kit<sup>-</sup>CD45<sup>+</sup> cells of all live cells have been noted. The portions of C-kit<sup>+</sup>CD45<sup>+</sup> and C-kit<sup>-</sup>CD45<sup>+</sup> cells of all live cells for several sample groups are, respectively, summarized in C and D. Mean, standard error of the mean (SEM), and individual data points are displayed. Group sample size is noted in parentheses following each x-axis label. Statistical comparisons between heart chambers, failing/nonfailing hearts, and ischemic/nonischemic failing hearts were conducted as described in *Statistics*. \* $P < 0.05$ ; \*\* $P < 0.01$ ; \*\*\* $P < 0.001$ . The percentages of false-positive cells based on isotype controls have been subtracted for the summary statistics in C and D, but not for the example FACS plots of A and B. HF, heart failure.

## The Transcriptome of C-kit<sup>+</sup>CD45<sup>+</sup> Mast Cells Differed Significantly in Comparison with C-kit<sup>-</sup>CD45<sup>+</sup> Hematopoietic Cells as well as between Failing and Nonfailing Hearts

FACS-sorted C-kit<sup>+</sup>CD45<sup>+</sup> and C-kit<sup>-</sup>CD45<sup>+</sup> samples underwent RNA sequencing followed by principal component analysis (PCA). C-kit<sup>+</sup>CD45<sup>+</sup> samples clustered separately from C-kit<sup>-</sup>CD45<sup>+</sup> samples in both failing (Fig. 3A) and nonfailing (Fig. 3B) hearts based on the first principal component (PC). C-kit<sup>+</sup>CD45<sup>+</sup> sample clustering based on the first PC correlated with high expression of mast cell marker genes, including tryptase (*TPSAB1/TPSB2*, Supplemental Fig. S3).

C-kit<sup>+</sup>CD45<sup>+</sup> samples from failing and nonfailing hearts clustered separately based on the first PC (Fig. 3C). C-kit<sup>-</sup>CD45<sup>+</sup> samples isolated from failing and nonfailing hearts also clustered based on the first PC (Fig. 3D). The clustering was, however, less distinct in comparison with that of the C-kit<sup>+</sup>CD45<sup>+</sup> samples.

C-kit<sup>+</sup>CD45<sup>+</sup> samples isolated from the respective heart chambers of failing hearts did not demonstrate significant clustering based on heart chamber origin (Supplemental Fig. S4).

### C-kit<sup>+</sup>CD45<sup>+</sup> Cells in Nonfailing Hearts Compared with C-kit<sup>-</sup>CD45<sup>+</sup> Cells Demonstrated Significant Activation of Pathways Associated with IL-33 Signaling, Prostaglandin/Thromboxane Synthesis, and Angiotensinogen to Angiotensin Metabolism

When C-kit<sup>+</sup>CD45<sup>+</sup> and C-kit<sup>-</sup>CD45<sup>+</sup> samples isolated from nonfailing hearts were compared, 381 genes were significantly differentially expressed at an adjusted *P* value < 0.05 (Supplemental Table S4). The mast cell marker genes *TPSAB1/TPSB2*, *KIT*, *CPA3*, and *HDC* were significantly higher expressed in C-kit<sup>+</sup>CD45<sup>+</sup> cells. The transcriptomic patterns of the two populations were compared using IPA pathway analysis, resulting in eight significantly enriched pathways (Fig. 4, Supplemental Table S5).

“IL-33 Signaling Pathway,” “synthesis of prostaglandins (PG) and thromboxanes (TX),” and “metabolism of angiotensinogen to angiotensin” constituted the significant pathways for which *Z*-scores could be determined and were all activated in C-kit<sup>+</sup>CD45<sup>+</sup> cells, that is, had *Z*-scores ≥ 2. For five significant pathways, no *Z*-score could be calculated.

### C-kit<sup>+</sup>CD45<sup>+</sup> Cells in Failing Hearts Compared with C-kit<sup>-</sup>CD45<sup>+</sup> Cells Demonstrated Significant Activation of Pathways Associated with Cardiac Hypertrophy, Fibrotic Diseases, Intercellular Signaling, and Immune Response

When C-kit<sup>+</sup>CD45<sup>+</sup> and C-kit<sup>-</sup>CD45<sup>+</sup> samples isolated from failing hearts were compared, 8,667 genes were significantly differentially expressed at an adjusted *P* value < 0.05 (Supplemental Table S6). The mast cell marker genes *TPSAB1/TPSB2*, *KIT*, *CPA3*, *HDC*, and *CMA1* were significantly higher expressed in C-kit<sup>+</sup>CD45<sup>+</sup> cells. The transcriptomic patterns of the two populations were compared using IPA pathway analysis, resulting in 97 significantly enriched pathways (Fig. 5, A and B, Supplemental Table S7). Most enriched pathways were activated in C-kit<sup>+</sup>CD45<sup>+</sup> cells, that is, had a *Z*-score ≥ 2.

C-kit<sup>+</sup>CD45<sup>+</sup> cells demonstrated significant activation for pathways within the “cardiac hypertrophy and cardiogenesis” and “fibrotic diseases” clusters (Fig. 5, B and C), including “cardiac hypertrophy signaling,” “factors promoting cardiogenesis in vertebrates,” “pulmonary fibrosis idiopathic signaling pathway,” and the “hepatic fibrosis signaling pathway.” Notably, the “activation of matrix metalloproteinases” pathway was also activated in C-kit<sup>+</sup>CD45<sup>+</sup> cells.

Pathways within the “immune response” cluster (Fig. 5, B and C), including “IL-17 signaling,” “IL-33 signaling pathway,” “leukocyte extravasation signaling,” “neuroinflammation signaling pathway,” and “production of nitric oxide and reactive oxygen species in macrophages” were also significantly activated in C-kit<sup>+</sup>CD45<sup>+</sup> cells.

C-kit<sup>+</sup>CD45<sup>+</sup> cells also demonstrated significant activation for pathways within the “intercellular signaling” cluster (Fig. 5, B and C), including “FGF signaling,” “Endothelin-1 signaling,” “Eicosanoid signaling,” “estrogen receptor signaling,” “EGF signaling,” and the “WNT/CA<sup>+</sup> pathway.” The “intrinsic prothrombin activation pathway” was also activated in C-kit<sup>+</sup>CD45<sup>+</sup> cells.

### C-kit<sup>+</sup>CD45<sup>+</sup> Cells in Failing Hearts Compared with Nonfailing Hearts Demonstrated Significant Activation of Pathways Associated with the Immune Response, Interleukins, Fibrotic Diseases, and Inter-/Intracellular Signaling

When C-kit<sup>+</sup>CD45<sup>+</sup> samples isolated from failing and nonfailing hearts were compared, 4,049 genes were significantly differentially expressed at an adjusted *P* value < 0.05 (Supplemental Table S8). The mast cell marker genes *TPSAB1/TPSB2*, *KIT*, *CPA3*, and *CMA1* were significantly higher expressed in C-kit<sup>+</sup>CD45<sup>+</sup> cells in failing hearts. The transcriptomic patterns of the two populations were compared using IPA pathway analysis, resulting in 65 significantly enriched pathways (Fig. 6, A and B, Supplemental Table S9). Most enriched pathways were activated in C-kit<sup>+</sup>CD45<sup>+</sup> cells isolated from failing hearts, that is, had a *Z*-score ≥ 2, whereas no significant pathways were deactivated in C-kit<sup>+</sup>CD45<sup>+</sup> cells isolated from failing hearts. For six significant pathways, no *Z*-score could be calculated. When C-kit<sup>-</sup>CD45<sup>+</sup> cells isolated from failing and nonfailing hearts were compared, no significantly enriched pathways were identified (data not shown).

C-kit<sup>+</sup>CD45<sup>+</sup> cells in failing hearts demonstrated significant activation for the “hepatic fibrosis signaling pathway” and the “pulmonary fibrosis idiopathic signaling pathway” within the “fibrotic diseases” cluster (Fig. 6, B and C). The “regulation of the epithelial mesenchymal transition by growth factors pathway” was also activated in C-kit<sup>+</sup>CD45<sup>+</sup> cells in failing hearts.

A number of pathways within the “interleukins” and “immune response” clusters were significantly activated in C-kit<sup>+</sup>CD45<sup>+</sup> cells in failing hearts (Fig. 6, B and C), including “IL-17A signaling in fibroblasts,” “role of IL-17F in allergic inflammatory airway diseases,” “interleukin-4 and interleukin-13 signaling,” “interleukin-10 signaling,” “role of JAK family kinases in IL-6 type cytokine signaling,” “other interleukin signaling,” “neutrophil degranulation,” and “acute phase response signaling.”

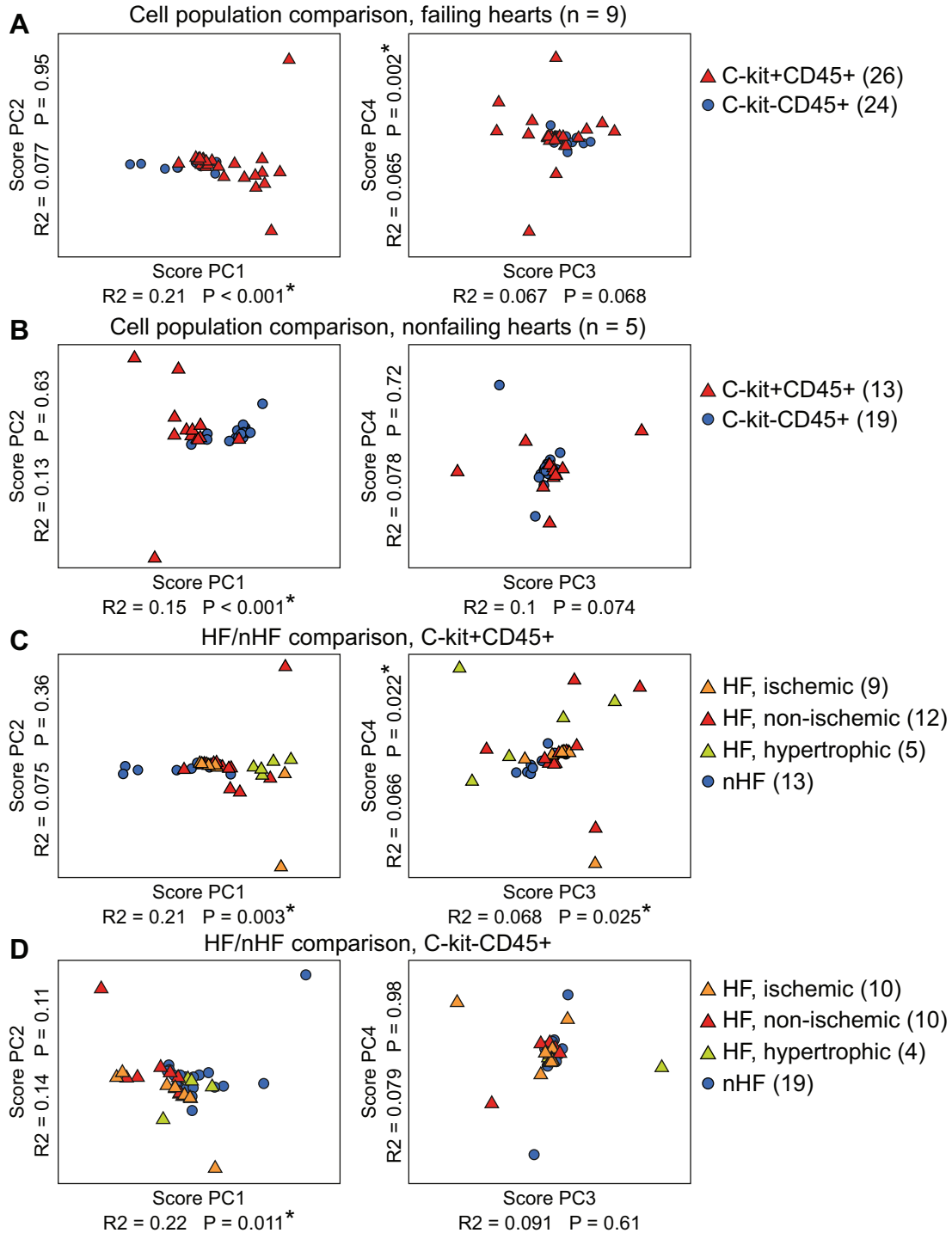


**Figure 3.** Clustering of isolated C-kit<sup>+</sup>CD45<sup>+</sup> and C-kit<sup>-</sup>CD45<sup>+</sup> samples based on the 5,000 genes with highest variance, visualized by principal component analysis (PCA). **A:** C-kit<sup>+</sup>CD45<sup>+</sup> samples compared with C-kit<sup>-</sup>CD45<sup>+</sup> samples in failing hearts. **B:** C-kit<sup>+</sup>CD45<sup>+</sup> samples compared with C-kit<sup>-</sup>CD45<sup>+</sup> samples in nonfailing hearts. **C:** C-kit<sup>+</sup>CD45<sup>+</sup> samples isolated from failing hearts compared with samples isolated from nonfailing hearts. **D:** C-kit<sup>-</sup>CD45<sup>+</sup> samples isolated from failing hearts compared with samples isolated from nonfailing hearts. A Kruskal–Wallis *H* test was conducted to assess the significance of clustering according to cell population identity (**A** and **B**) or presence/absence of heart failure (**C** and **D**) for each PC. *P* values < 0.05 have been noted with “\*.” Group sample size is noted within parentheses to the right of each group label, including all samples that were collected from each heart and included in the transcriptomic analysis (i.e., samples from the different chambers of each heart). HF, heart failure; nHF, not heart failure; PC, principal component.

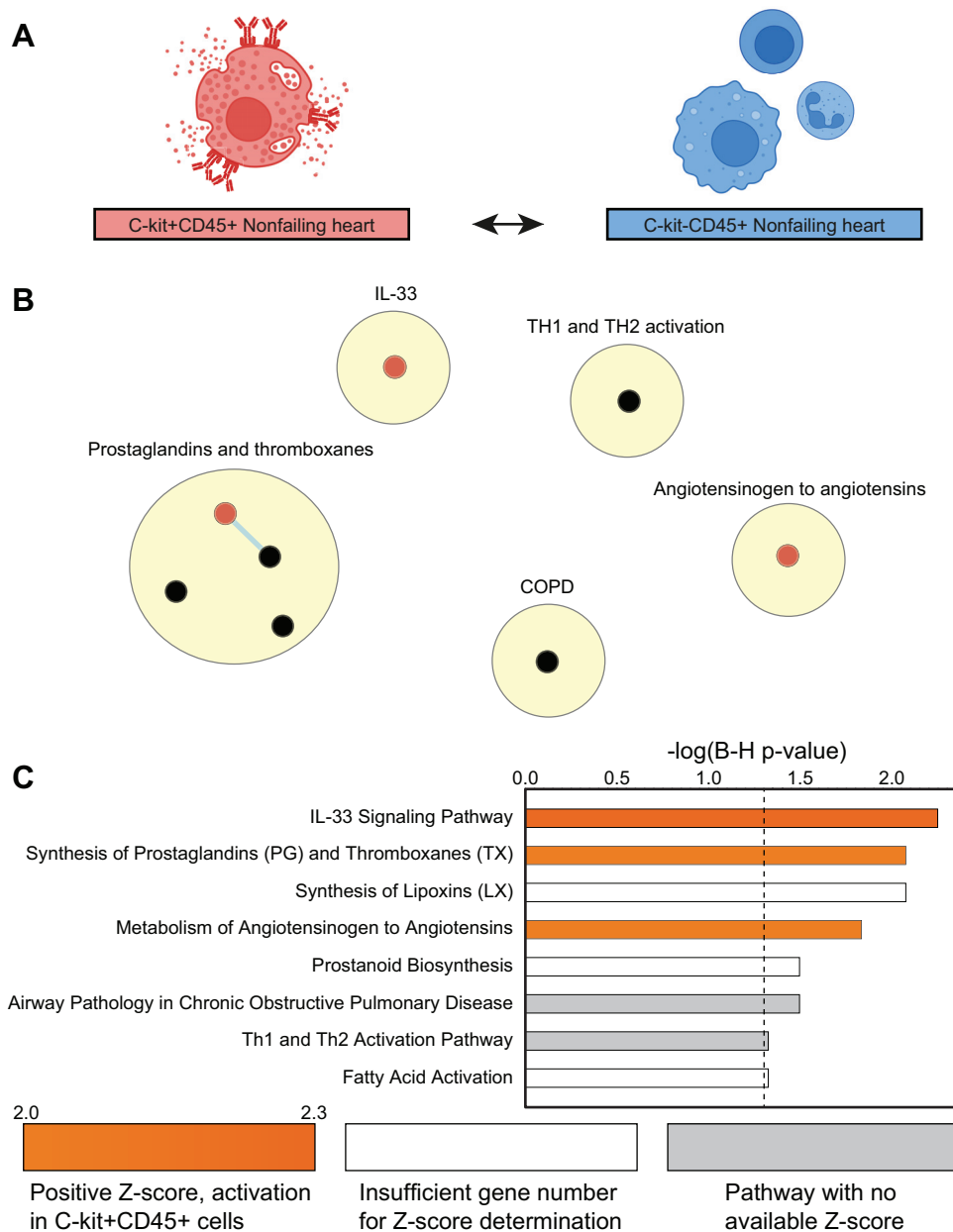


**Figure 4.** Analysis of activated/deactivated IPA pathways in C-kit<sup>+</sup>CD45<sup>+</sup> CMCs compared with C-kit<sup>-</sup>CD45<sup>+</sup> cells within non-failing donor hearts. **A:** analysis overview and color code for pathway visualization. **B:** significant pathways, that is, pathways with FDR-adjusted overlap *P* values ≤ 0.05 and absolute Z-scores ≥ 2 were visualized using Cytoscape. Pathways with undetermined Z-scores were also included if they had an FDR-adjusted overlap *P* value ≤ 0.05. Each node constituted one pathway and was color-coded according to activation status/Z-score. Red = activation in C-kit<sup>+</sup>CD45<sup>+</sup> CMCs (Z-score ≥ 2); blue = activation in C-kit<sup>-</sup>CD45<sup>+</sup> cells (Z-score ≤ -2); black = undetermined Z-score. The size of each node corresponds to the gene set size of the pathway. Biologically associated pathways were organized into clusters with names summarizing the biological relevance of the pathways. **C:** visualization of the most biologically relevant pathways included in the Cytoscape network. Bar size corresponds to the -log(Benjamini-Hochberg-adjusted *P* value) and color gradient to the Z-score. Dotted threshold line corresponds to a Benjamini-Hochberg-adjusted *P* value = 0.05. Orange = Z-score ≥ 2, that is, activated pathway in C-kit<sup>+</sup>CD45<sup>+</sup> CMCs; white = undetermined Z-score due to insufficient number of pathway-genes within the dataset; gray = undetermined Z-score due to the design of the pathway. B-H, Benjamini-Hochberg; CMCs, intracardiac mast cells; COPD, chronic obstructive pulmonary disease; IPA, ingenuity pathway analysis. Figure created with a licensed version of BioRender.com.

C-kit<sup>+</sup>CD45<sup>+</sup> cells in failing hearts demonstrated significant activation for several pathways within the “intercellular signaling” cluster (Fig. 6, B and C), that is, the “eicosanoid signaling,” “estrogen receptor signaling,” “extra-nuclear estrogen signaling,” “ephrin receptor signaling,” and “metabolism of nitric oxide: NOS3 activation and regulation” pathways. Pathways within the “intracellular signaling” cluster were also activated, including “P38 MAPK signaling,” “ERK/MAPK signaling,” “PIP3 activates AKT signaling,” and “HIF1 $\alpha$  signaling.”

**C-kit<sup>+</sup>CD45<sup>+</sup> Cells in Failing Hearts Demonstrated Activated Upstream Regulatory Elements Involved in Immunological and Fibrotic Signaling Compared with C-kit<sup>+</sup>CD45<sup>+</sup> Cells in Nonfailing Hearts**

IPA was used to predict upstream regulators (UREs) based on DEGs between C-kit<sup>+</sup>CD45<sup>+</sup> samples isolated from

failing and nonfailing hearts (Fig. 7, Supplemental Table S10). Seventy-nine UREs were significant, that is, activated with a Z-score > 3 or deactivated with a Z-score < -3 for C-kit<sup>+</sup>CD45<sup>+</sup> cells in failing hearts. Most of the 79 significant UREs were predicted to be activated in failing hearts (*n* = 63).

A large portion of the 79 UREs was associated with leukocyte function based on IPA disease and function analysis, that is, the UREs were included in the annotation terms “Inflammatory response” (*n* = 40), “Proliferation of immune cells” (*n* = 38), “Leukocyte migration” (*n* = 42), “Cell death of immune cells” (*n* = 37), and/or “Synthesis of eicosanoid” (*n* = 27). A portion of UREs was also included in annotation terms associated with cardiac pathophysiology and heart failure, that is, “Cardiomyopathy” (*n* = 36), “Hypertrophy of cardiac muscle” (*n* = 16), “Cell death of cardiomyocytes” (*n* = 18), and/or “Fibrosis of heart” (*n* = 17). URE-targeting drugs

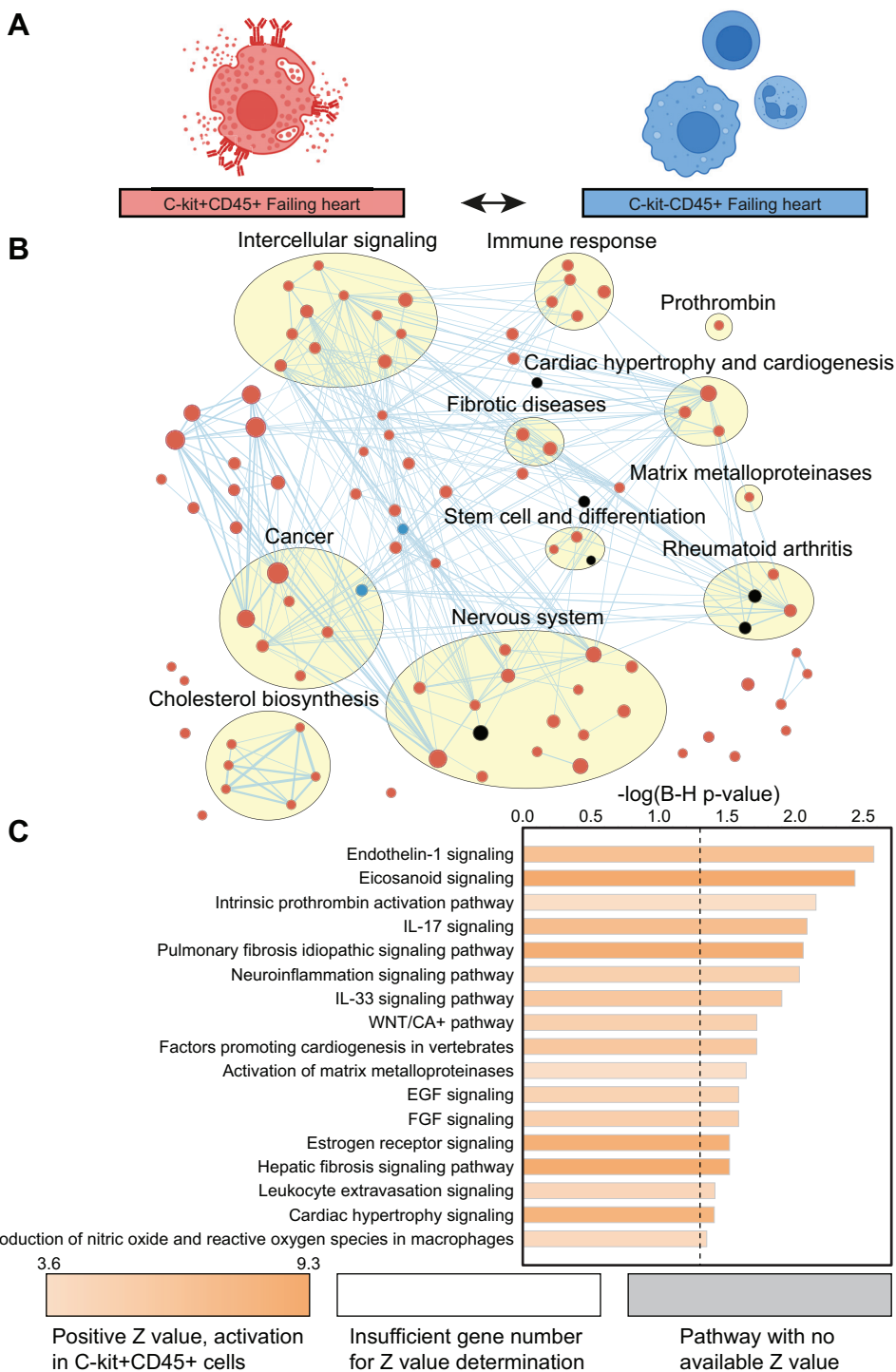


**Figure 5.** Analysis of activated/deactivated IPA pathways in C-kit<sup>+</sup>CD45<sup>+</sup> CMCs compared with C-kit<sup>-</sup>CD45<sup>+</sup> cells within failing hearts. **A:** analysis overview and color code for pathway visualization. **B:** significant pathways, that is, pathways with FDR-adjusted overlap *P* values ≤ 0.05 and absolute Z-scores ≥ 2 were visualized using Cytoscape. Pathways with undetermined Z-scores were also included if they had an FDR-adjusted overlap *P* value ≤ 0.05. Each node constituted one pathway and was color-coded according to activation status/Z-score. Red = activation in C-kit<sup>+</sup>CD45<sup>+</sup> CMCs (Z-score ≥ 2); blue = activation in C-kit<sup>-</sup>CD45<sup>+</sup> cells (Z-score ≤ -2); black = undetermined Z-score. The size of each node corresponds to the gene set size of the pathway. Biologically associated pathways were organized into clusters with names summarizing the biological relevance of the pathways. **C:** visualization of the most biologically relevant pathways included in the Cytoscape network. Bar size corresponds to the  $-\log(\text{Benjamini-Hochberg-adjusted } P \text{ value})$  and color gradient to the Z-score. Dotted threshold line corresponds to a Benjamini-Hochberg-adjusted *P* value = 0.05. All pathways within the diagram had Z-scores ≥ 2, that is, activated in C-kit<sup>+</sup>CD45<sup>+</sup> CMCs, and were color-coded orange. B-H, Benjamini-Hochberg; CMCs, intracardiac mast cells; COPD, chronic obstructive pulmonary disease; IPA, ingenuity pathway analysis. Figure created with a licensed version of BioRender.com.

were identified for 35 UREs based on the IPA Knowledge Base.

## DISCUSSION

In the current study, human C-kit<sup>+</sup>CD45<sup>+</sup> cardiac mast cells (CMCs) were identified in all chambers of failing and nonfailing hearts. CMCs in failing human hearts demonstrated a large number of activated pathways compared

with CMCs in nonfailing hearts, as well as to C-kit<sup>-</sup>CD45<sup>+</sup> hematopoietic cells in failing hearts (Fig. 8). Many activated pathways were associated with tissue fibrosis, remodeling, and inflammatory signaling. Seventy-nine upstream regulatory elements (UREs) were identified, most of which were activated in CMCs in failing hearts compared with nonfailing hearts. A large portion of activated UREs were associated with leukocyte function, synthesis of eicosanoids, and/or heart failure-associated processes such as heart fibrosis,

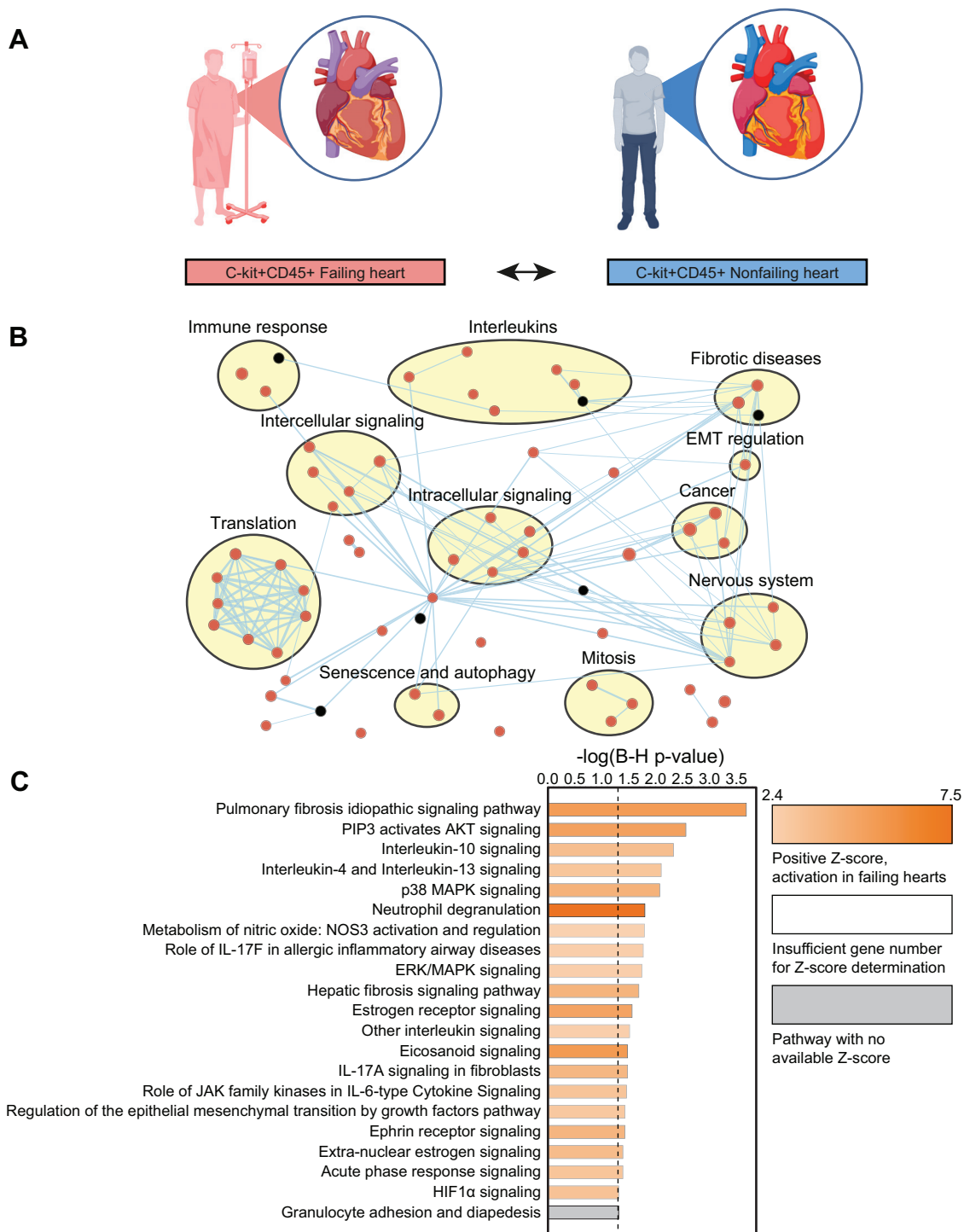


**Figure 6.** Analysis of activated/deactivated IPA pathways in C-kit<sup>+</sup>CD45<sup>+</sup> CMCs in failing hearts compared with C-kit<sup>+</sup>CD45<sup>+</sup> CMCs in nonfailing donor hearts. **A:** analysis overview and color code for pathway visualization. **B:** significant pathways, that is, pathways with FDR-adjusted overlap *P* values  $\leq 0.05$  and absolute Z-scores  $\geq 2$  were visualized using Cytoscape. Pathways with undetermined Z-scores were also included if they had an FDR-adjusted overlap *P* value  $\leq 0.05$ . Each node constituted one pathway and was color-coded according to activation status/Z-score. Red = activation in C-kit<sup>+</sup>CD45<sup>+</sup> CMCs in failing hearts (Z-score  $\geq 2$ ); blue = activation in C-kit<sup>+</sup>CD45<sup>+</sup> cells in nonfailing donor hearts (Z-score  $\leq -2$ ); black = undetermined Z-score. The size of each node corresponds to the gene set size of the pathway. Biologically associated pathways were organized into clusters with names summarizing the biological relevance of the pathways. **C:** visualization of the most biologically relevant pathways included in the Cytoscape network. Bar size corresponds to the  $-\log(\text{Benjamini-Hochberg-adjusted } P \text{ value})$  and color gradient to the Z-score. Dotted threshold line corresponds to a Benjamini-Hochberg-adjusted *P* value = 0.05. Orange = Z-score  $\geq 2$ , that is, activated pathway in C-kit<sup>+</sup>CD45<sup>+</sup> CMCs in failing hearts; gray = undetermined Z-score due to the design of the pathway. B-H, Benjamini-Hochberg; CMCs, intracardiac mast cells; COPD, chronic obstructive pulmonary disease; IPA, ingenuity pathway analysis. Figure created with a licensed version of BioRender.com.

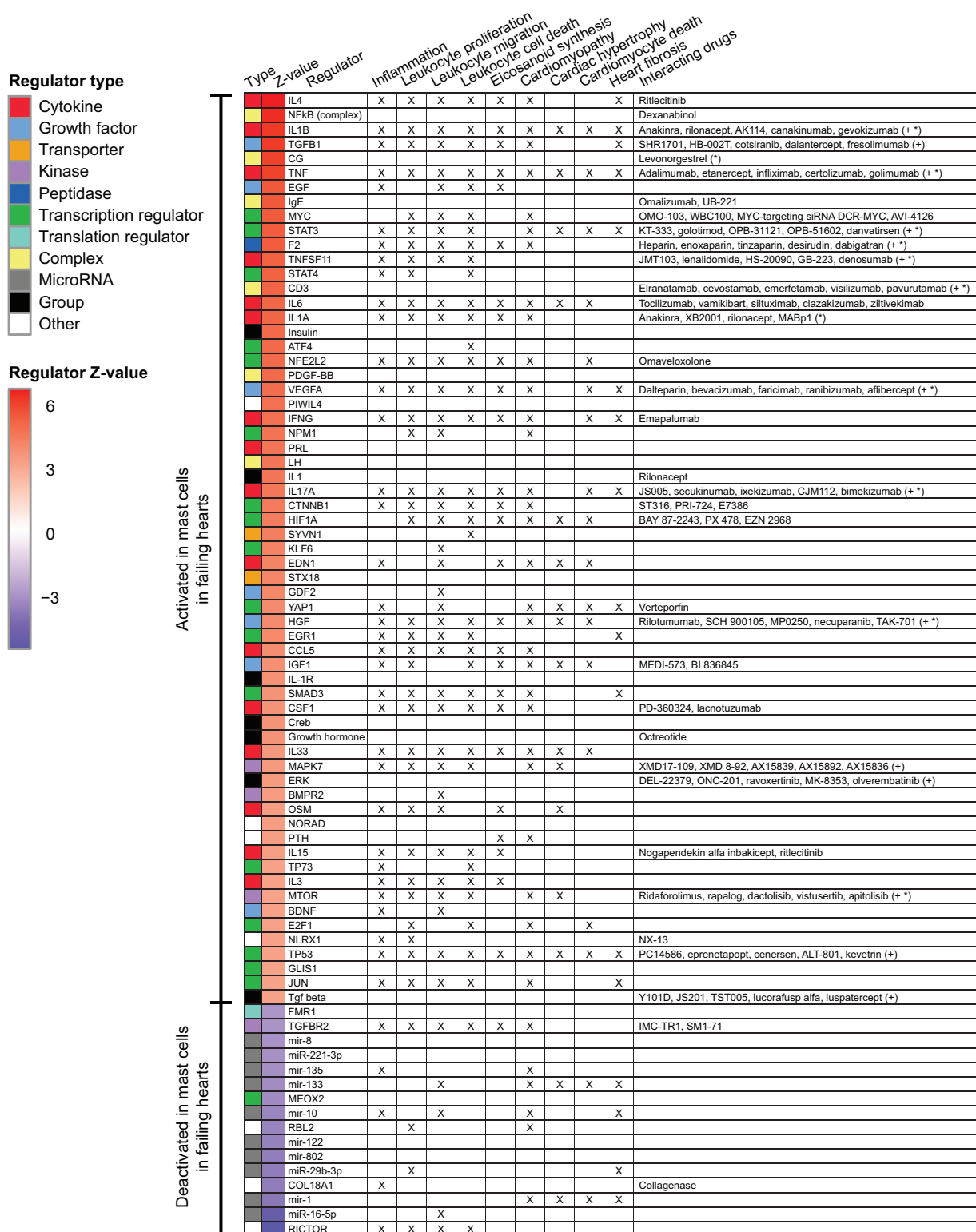


**Figure 7.** Predicted upstream regulators (UREs) and interacting drugs. IPA was used to predict UREs based on DEGs between C-kit<sup>+</sup> CD45<sup>+</sup> samples isolated from nonfailing and failing hearts. UREs with a Z-score > 3 or < -3 were visualized in a heatmap. URE type is noted to the left of the heatmap. Functional URE annotations were identified based on the IPA database and noted with an “X” in the columns to the right of the heatmap. Functional annotation terms were abbreviated for visualization. URE-interacting drugs according to the IPA database have also been noted. In cases where combinations of drugs are known to interact with the URE, this has been marked by “(+)”. For UREs with >5 known interacting drugs, up to five examples of drugs have been noted, followed by “(+)”. DEGs, differentially expressed genes; IPA, ingenuity pathway analysis.

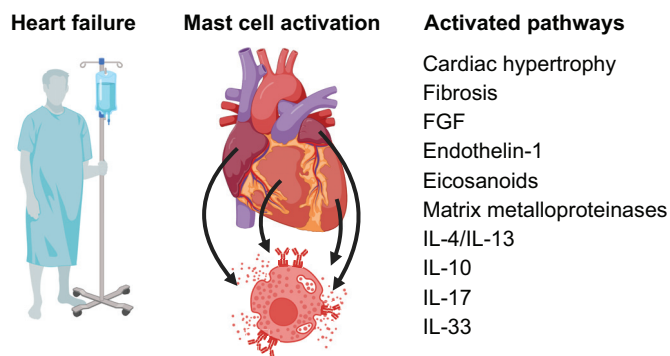


**Figure 8.** Summary of study findings. Figure created with a licensed version of BioRender.com.

hypertrophy, and cell death of cardiomyocytes. UREs may constitute candidates for CMC modulation through URE-targeting drugs.

### Cardiac Mast Cells Exist in All Chambers of Failing and Nonfailing Human Hearts

The presence of CMCs within all heart chambers indicates that mast cells may contribute to physiologic and pathophysiological processes in the entire human heart. Notably, the smaller portion of CMCs within the left ventricle corroborated the atrial enrichment of CMCs previously observed in humans (7) and mice (4). Although the cause for the atrial and right ventricular enrichment of CMCs observed in the current study is not known, the transcriptomic analysis conducted in the current study indicates that the phenotypes of atrial and ventricular CMCs are similar.

In contrast to our results, previous studies have observed an increased CMC density in failing compared with nonfailing human hearts (16–18). Notably, these studies have been limited to histological/immunohistochemical analyses of ventricular biopsies and have mainly implemented either toluidine blue/alcian blue or staining for mast cell-associated tryptase/chymase, rather than C-kit, for identification of mast cells. The reasons for the discrepancy between previous studies and the current study are unclear, but could potentially be differences in methodology, study participant cohorts and/or study power. Interestingly, maturation of immature CMCs rather than expansion of the total CMC population may explain the increased CMC density observed following acute volume overload in rats (26), as well as in spontaneously hypertensive rats (27). As immature hematopoietic cells retain their C-kit expression during maturation into tissue-resident mast cells, both immature and mature mast cells should be identified as C-kit<sup>+</sup>. Sperr et al. (7) found that C-kit was expressed by most CMCs, supporting identification of CMCs based on C-kit positivity. Due to the heterogeneity of the CMC population, correlation between disease state and mast cell concentration may not adequately reflect the pathophysiological contribution of CMCs. CMC gene and/or protein expression therefore needs to be taken into account.

### Mast Cells in Failing Hearts Are Characterized by a Distinct Transcriptomic Activation Pattern

C-kit<sup>+</sup>CD45<sup>+</sup> CMCs clustered distinctly compared with C-kit<sup>-</sup>CD45<sup>+</sup> hematopoietic cells in both failing and non-

failing hearts based on PCA. The number of significantly differentially expressed genes (DEGs) and enriched pathways based on the C-kit<sup>+</sup>CD45<sup>+</sup>/C-kit<sup>-</sup>CD45<sup>+</sup> comparison was considerably larger in failing hearts than in nonfailing hearts. Bootstrapping modeling demonstrated that limited study power was not a likely explanation for the observed differences in pathway activation patterns between failing and nonfailing hearts (data not shown). A more likely explanation may be differential activation of CMCs and the bulk of hematopoietic cells in the failing human heart. These results are in support of a particular pathophysiological importance for CMCs in human heart failure.

### Activation of Fibrosis-Associated Pathways in Cardiac Mast Cells in Failing Hearts

Both pro- and antifibrotic roles of CMCs have been described previously (28). These discrepancies may relate to context-dependent effects of CMCs as well as methodological differences, including the use of different genetic models of mast cell deficiency. The role of CMCs in cardiac remodeling and fibrosis remains incompletely understood, particularly as human CMCs have scarcely been investigated (28).

In the current study, C-kit<sup>+</sup>CD45<sup>+</sup> CMCs in failing hearts demonstrated significant activation for several fibrosis-associated pathways, both compared with C-kit<sup>-</sup>CD45<sup>+</sup> cells in failing hearts and to C-kit<sup>+</sup>CD45<sup>+</sup> CMCs in nonfailing hearts. Furthermore, 13 UREs, which were significantly activated in CMCs in failing hearts, have been implicated in heart fibrosis, including IL-4, IL-1 $\beta$ , TGF- $\beta$ 1, TNF, and IL-17A (29). These results were in line with previous observations of a positive correlation between CMC density and fibrosis in the human heart (17, 18). Furthermore, animal models of cardiac pressure overload (5, 13) and myocarditis (9, 14) have suggested that mast cells may contribute to profibrotic signaling, including via tryptase, chymase, and bFGF.

As the “FGF signaling” pathway was activated in C-kit<sup>+</sup>CD45<sup>+</sup> CMCs compared with C-kit<sup>-</sup>CD45<sup>+</sup> cells in failing hearts, our results are in line with CMC-mediated profibrotic FGF signaling in human heart failure. “Endothelin-1 signaling” constitutes a profibrotic and proinflammatory pathway previously implicated in cardiac remodeling and heart failure (29), and was associated with C-kit<sup>+</sup>CD45<sup>+</sup> CMCs in failing hearts in the current study. Interestingly, endothelin-1 has previously been implicated in mast cell degranulation, MMP2 activation, decreased collagen volume and ventricle dilation in rat hearts (30). CMC-mediated endothelin-1 signaling could possibly result in both autocrine and paracrine effects in the failing heart.

C-kit<sup>+</sup>CD45<sup>+</sup> CMCs in failing hearts demonstrated activation of the “activation of matrix metalloproteinases” (MMPs) pathway compared with C-kit<sup>-</sup>CD45<sup>+</sup> cells. Expression of MMPs by mast cells (3) as well as MMP activation by mast cell-associated chymase (31) and tryptase (32) have been reported previously. In the current study, significantly higher expression of tryptase (*TPSAB1/TPSB2*) and chymase (*CMA1*) was observed for C-kit<sup>+</sup>CD45<sup>+</sup> CMCs when compared with C-kit<sup>-</sup>CD45<sup>+</sup> hematopoietic cells in failing hearts as well as to C-kit<sup>+</sup>CD45<sup>+</sup> CMCs in nonfailing hearts. CMC-dependent activation of MMP2 has been implicated in extracellular matrix remodeling (ECM) and collagen

degradation following aortocaval fistulation (33) and mitral regurgitation (8). Our results support a role for CMC mediated MMP activation and ECM remodeling in the failing human heart.

Mast cells have been suggested to contribute to renin-angiotensin-mediated cardiac remodeling and fibrosis by expressing renin (34), as well as by secreting chymase (35) and cathepsin g (36), which in turn may convert angiotensin I to angiotensin II. Although the “metabolism of angiotensinogen to angiotensin” pathway was activated in C-kit<sup>+</sup>CD45<sup>+</sup> CMCs compared with C-kit<sup>-</sup>CD45<sup>+</sup> cells in nonfailing hearts, no similar significant activation was observed for C-kit<sup>+</sup>CD45<sup>+</sup> CMCs in failing hearts. Chymase (*CMA1*) as well as cathepsin g (*CTSG*) were, however, significantly higher expressed by C-kit<sup>+</sup>CD45<sup>+</sup> CMCs in failing hearts when compared with C-kit<sup>-</sup>CD45<sup>+</sup> hematopoietic cells in failing hearts as well as to C-kit<sup>+</sup>CD45<sup>+</sup> CMCs in nonfailing hearts. Notably, renin (*REN*) was also significantly higher expressed by C-kit<sup>+</sup>CD45<sup>+</sup> CMCs in failing hearts when compared with C-kit<sup>-</sup>CD45<sup>+</sup> hematopoietic cells. CMCs may, therefore, possibly contribute to local renin-angiotensin signaling in the failing human heart.

Several IL-17-associated signaling pathways were activated in C-kit<sup>+</sup>CD45<sup>+</sup> CMCs in failing hearts. Furthermore, IL-17A was identified as an activated URE in CMCs in failing hearts, suggesting that IL-17 signaling may act both up- and downstream of CMCs. Notably, IL-17 has generally been described as a proinflammatory and profibrotic cytokine that may contribute to cardiac injury, cardiomyocyte apoptosis, leukocyte recruitment, and increased release of reactive oxygen/nitrogen species and cytokines (37). IL-17 signaling has been reported to be involved in cardiac remodeling and fibrosis following myocardial infarction and myocarditis (37, 38).

### Activated Th2-Associated Interleukin Signaling Pathways in Cardiac Mast Cells—Beneficial or Deleterious in Heart Failure?

Compared with CMCs in nonfailing hearts, CMCs in failing hearts demonstrated significant activation of pathways associated with IL-4/IL-13 and IL-10. Notably, the “IL-33 signaling pathway” was activated in C-kit<sup>+</sup>CD45<sup>+</sup> CMCs compared with C-kit<sup>-</sup>CD45<sup>+</sup> cells both in nonfailing and failing hearts. Activated UREs in CMCs in failing hearts included IL-4 and IL-33. These interleukins have previously been associated with the Th2 immune response, anti-inflammatory signaling, and either attenuated or stimulated fibrosis. Several cardioprotective effects of IL-33 have been observed in models of myocardial infarction, ischemia/reperfusion injury, and cardiac remodeling, including improved cardiomyocyte viability and decreased cardiac fibrosis and hypertrophy (28, 39). IL-33 is known to inhibit the Th1 and stimulate the Th2 immune response, including activation of mast cells and expression of Th2 response-associated cytokines such as IL-4, IL-10, and IL-13 (39). Activated mast cells may secrete IL-13, which has been reported to inhibit proinflammatory cytokine expression (28) and contribute to fibrosis, at least in noncardiac organ systems (40). Cardioprotective effects of IL-13 following myocardial infarction has been suggested, including induction of an anti-inflammatory and efferocytotic macrophage subpopulation

(41). The role of IL-13 in cardiac remodeling and fibrosis, however, remains insufficiently understood (29). IL-4 signaling may have both anti-inflammatory and profibrotic effects (29, 42). Stimulation of mast cells with IL-4 has also been shown to result in activation and proliferation, in part mediated through downstream leukotriene signaling (43). Furthermore, IL-4 is known to be expressed by mast cells, and mast cell inhibition has been associated with attenuated cardiac fibrosis and decreased cardiac IL-4 levels in spontaneously hypertensive rats (13). IL-10 has, overall, been suggested to mediate cardioprotective effects, including an attenuation of inflammation, oxidative stress, apoptosis and TNF-alpha signaling (42). Results have, however, varied between studies, and both pro- and antifibrotic effects of IL-10 signaling have been reported (29).

Taken together, our results indicate that CMCs in failing human hearts may be involved in multiple up- and/or downstream signaling systems with potentially beneficial effects, including IL-4, IL-10, IL-13, and IL-33. In support of a protective role of CMC signaling pathways, Kwon et al. (12) found that granules isolated from peritoneal mast cells caused increased angiogenesis and macrophage infiltration, as well as attenuated fibrosis and remodeling and when administered during the acute phase of ischemia/reperfusion injury in rats. The effects of CMCs in the failing heart may thus be complex and warrant further functional studies.

### Eicosanoid Signaling Pathways Are Activated in Cardiac Mast Cells

The “eicosanoid signaling” pathway was significantly activated in C-kit<sup>+</sup>CD45<sup>+</sup> CMCs in failing hearts, both compared with C-kit<sup>-</sup>CD45<sup>+</sup> cells in failing hearts and C-kit<sup>+</sup>CD45<sup>+</sup> CMCs in nonfailing hearts. Furthermore, the “synthesis of prostaglandins (PG) and thromboxanes (TX)” pathway was activated in C-kit<sup>+</sup>CD45<sup>+</sup> CMCs in nonfailing hearts compared with C-kit<sup>-</sup>CD45<sup>+</sup> cells in nonfailing hearts. Mast cells are known to produce eicosanoid substances including prostaglandin (PG) D<sub>2</sub> and leukotrienes (LT) B<sub>4</sub>/C<sub>4</sub>/D<sub>4</sub>/E<sub>4</sub> (3). These eicosanoids have mainly been implicated as contributing factors in allergic diseases and the type 2 immune response (3, 43, 44). PGD<sub>2</sub> and LTC<sub>4</sub>/C<sub>4</sub>/D<sub>4</sub>/E<sub>4</sub> signaling may stimulate cytokine signaling, leukocyte chemotaxis, vasodilation, and vascular permeability (3, 43, 44). Interestingly, mast cell-secreted eicosanoids may also have autocrine stimulating effects on mast cell proliferation, chemotaxis, production of Th2-associated cytokines, and degradation (43).

Although results have varied between studies, deleterious effects of eicosanoid signaling have been suggested in myocardial infarction and ischemia/reperfusion injury, and both PGD<sub>2</sub> and LTC<sub>4</sub> may induce cardiomyocyte apoptosis (45–47). Prostaglandin D synthase expression was recently reported to be elevated in CMCs in patients with Duchenne muscular dystrophy-associated cardiomyopathy (48). Furthermore, PGD<sub>2</sub> was elevated in combination with several other eicosanoid species in failing mouse hearts (49) and predicted 1-year mortality following acute decompensation of heart failure in combination with other arachidonic acid-derived substances (50). Although eicosanoids may play a role in cardiac disease, effects of

eicosanoids produced by CMCs in failing human hearts have not yet been extensively characterized. Based on the activation of eicosanoid signaling in the current study, CMC eicosanoid signaling in failing hearts should be further studied. Notably, 26 significantly activated UREs in CMCs in failing hearts were found to be associated with synthesis of eicosanoids, and may, therefore, constitute important regulators of CMC eicosanoid signaling.

### Limitations

Some study limitations should be noted. The scarcity of available failing and nonfailing hearts for study inclusion resulted in a relatively limited sample size. Study power may, as a result, have been too limited to detect modest differences between groups.

A small number of female study participants was included in the study. This was likely caused by random sampling, as participants were included regardless of sex. Due to the low number of female study participants, no analysis of possible sex-specific effects on CMC biology could be conducted. Whether clinical parameters, such as comorbidities or treatment with LVAD, may affect the transcriptomic pattern of mast cells was also beyond the scope of this study.

Although samples isolated from failing hearts with different etiologies tended to cluster distinctly, the sample size was too limited to enable any transcriptomic comparison of CMCs in ischemic, nonischemic and hypertrophic heart failure. Further studies are, therefore, needed to compare the transcriptomic patterns of CMCs in different heart failure populations.

Hearts of organ donors were included in the study as a control group. Although none of the donors suffered from chronic heart failure, most had been disqualified from transplantation either due to high age or comorbidities. Completely healthy organ donor hearts are, however, generally unavailable for research purposes due to their use in heart transplantation.

Flow cytometric analysis and sorting were limited to C-kit<sup>+</sup>CD45<sup>+</sup> CMCs and C-kit<sup>-</sup>CD45<sup>+</sup> hematopoietic cells. Analysis of specific subsets of nonmast hematopoietic cell populations, such as macrophages and lymphocytes, was, unfortunately, beyond the scope of the current study.

Proteomic as well as functional studies were beyond the scope of the current study, in part due to the limited amount of biopsy tissue available for study. The various CMC-associated mechanisms that have been suggested based on the study results need to be assessed through further proteomic and functional studies. As several animal models previously used in the study of CMCs have been associated with important study limitations (28, 51), functional in vitro studies should preferably be aimed at CMCs isolated from human hearts or mature mast cells derived from human extra-cardiac sources.

### Conclusions

Cardiac mast cells were identified in all chambers of failing and nonfailing human hearts. In failing hearts, mast cells demonstrated significant transcriptomic activation for multiple signaling pathways involved in fibrosis, inflammation, and cardiac remodeling. Activated upstream regulators of

cardiac mast cells in failing hearts were associated with leukocyte function and heart failure-associated processes such as heart fibrosis, hypertrophy, and cardiomyocyte cell death. The transcriptomic activation pattern suggests that cardiac mast cells may have a pathophysiological role in human heart failure.

### DATA AVAILABILITY

Source data for this study are openly available through a sample information file and a processed RNA-seq raw counts file at <https://doi.org/10.6084/m9.figshare.30666515>. For output data from differential gene expression, IPA canonical pathway, and IPA upstream regulator analyses, see Supplemental Material.

### SUPPLEMENTAL MATERIAL

Supplemental Figs. S1–S4: <https://doi.org/10.6084/m9.figshare.30666212>.

Supplemental Tables S1–S10: <https://doi.org/10.6084/m9.figshare.30666281>.

### ACKNOWLEDGMENTS

The authors thank the Cell and Tissue laboratory as well as the coordinators at the centrum for transplantation, Sahlgrenska University Hospital, for assistance with the logistics and the administration of the donor tissues. The authors thank the nurses and surgeons at the Department of Cardiothoracic Surgery, Sahlgrenska University Hospital, for skillful handling of the biopsies.

The laboratory work underlying this article was conducted at the Department of Laboratory Medicine, Institute of Biomedicine, Sahlgrenska Academy, University of Gothenburg, Gothenburg, Sweden.

Figures 1, 4, 5, 6, and 8 and graphical abstract created with a licensed version of BioRender.com [Sandstedt, M. (2026) <https://BioRender.com/Ob9o447>; <https://BioRender.com/xilza8t>; <https://BioRender.com/97jsh9j>; <https://BioRender.com/gnxkdpd>; <https://BioRender.com/whnjzbu>; <https://BioRender.com/nztm4x7>].

### GRANTS

This work was supported by grants from the Swedish Society of Medicine (to J. Sandstedt), the Gothenburg Society of Medicine (to M.S.), the Heart-Lung Foundation (to L.M.H.), the Emelle Foundation (to M.S.), the foundations of the Sahlgrenska University Hospital (to M.S.), the University of Skövde (to J. Synnergren), and ALF research grants from the Sahlgrenska University Hospital (to L.M.H.).

### DISCLOSURES

No conflicts of interest, financial or otherwise, are declared by the authors.

### AUTHOR CONTRIBUTIONS

Mikael Sandstedt, L.M.H., G.D., A.J., J. Synnergren, and J. Sandstedt conceived and designed research; Mikael Sandstedt, M. Jonsson, K.V., Maria Sandstedt, G.D., A.J., and J. Sandstedt performed experiments; Mikael Sandstedt, M. Johansson, B.U., L.M.H., V.R.S., J. Synnergren, and J. Sandstedt analyzed data; Mikael Sandstedt, M. Johansson, B.U., L.M.H., V.R.S., J. Synnergren, and J. Sandstedt interpreted results of experiments; Mikael Sandstedt

and J. Sandstedt prepared figures; Mikael Sandstedt and J. Sandstedt drafted manuscript; Mikael Sandstedt, M. Johansson, M. Jonsson, K.V., B.U., Maria Sandstedt, L.M.H., V.R.S., G.D., A.J., J. Synergren, and J. Sandstedt edited and revised manuscript; Mikael Sandstedt, M. Johansson, M. Jonsson, K.V., B.U., Maria Sandstedt, L.M.H., V.R.S., G.D., A.J., J. Synergren, and J. Sandstedt approved final version of manuscript.

## REFERENCES

- Savarese G, Becher PM, Lund LH, Seferovic P, Rosano GMC, Coats AJS. Global burden of heart failure: a comprehensive and updated review of epidemiology. *Cardiovasc Res* 118: 3272–3287, 2023 [Erratum in *Cardiovasc Res* 119: 1453, 2023]. doi:10.1093/cvr/cvac013.
- McDonagh TA, Metra M, Adamo M, Gardner RS, Baumbach A, Böhm M, Burri H, Butler J, Celutkienė J, Chioncel O, Cleland JGF, Coats AJS, Crespo-Leiro MG, Farmakis D, Gilard M, Heymans S, Hoes AW, Jaarsma T, Jankowska EAJ, Lainscak M, Lam CSP, Lyon AR, McMurray JJV, Mebazaa A, Mindham R, Muneretto C, Piepoli MF, Price S, Rosano GMC, Ruschitzka F, Ruschitzka AK; ESC Scientific Document Group. 2021 ESC guidelines for the diagnosis and treatment of acute and chronic heart failure: developed by the task force for the diagnosis and treatment of acute and chronic heart failure of the European Society of Cardiology (ESC). With the special contribution of the Heart Failure Association (HFA) of the ESC. *Eur Heart J* 42: 3599–3726, 2021 [Erratum in *Eur Heart J* 42: 4901, 2021]. doi:10.1093/eurheartj/ehab368.
- Elieh Ali Komi D, Wöhrl S, Bielory L. Mast cell biology at molecular level: a comprehensive review. *Clin Rev Allergy Immunol* 58: 342–365, 2020. doi:10.1007/s12016-019-08769-2.
- Ingason AB, Mechet F, Atacho DAM, Steingrímsson E, Petersen PH. Distribution of mast cells within the mouse heart and its dependency on Mif. *Mol Immunol* 105: 9–15, 2019. doi:10.1016/j.molimm.2018.11.009.
- Shiota N, Rysa J, Kovanen PT, Ruskoaho H, Kokkonen JO, Lindstedt KA. A role for cardiac mast cells in the pathogenesis of hypertensive heart disease. *J Hypertens* 21: 1935–1944, 2003. doi:10.1097/00004872-200310000-00022.
- Stamenov N, Kotov G, Iliev A, Landzhov B, Kirkov V, Stanchev S. Mast cells and basic fibroblast growth factor in physiological aging of rat heart and kidney. *Biotech Histochem* 97: 504–518, 2022. doi:10.1080/10520295.2021.2024251.
- Sperr WR, Bankl HC, Mundigler G, Klappacher G, Grossschmidt K, Agis H, Simon P, Laufer P, Imhof M, Radaszkiewicz T, Glogar D, Lechner K, Valent P. The human cardiac mast cell: localization, isolation, phenotype, and functional characterization. *Blood* 84: 3876–3884, 1994.
- Stewart JA Jr, Wei CC, Brower GL, Rynders PE, Hankes GH, Dillon AR, Lucchesi PA, Janicki JS, Dell’Italia LJ. Cardiac mast cell- and chymase-mediated matrix metalloproteinase activity and left ventricular remodeling in mitral regurgitation in the dog. *J Mol Cell Cardiol* 35: 311–319, 2003. doi:10.1016/s0022-2828(03)00013-0.
- Palaniyandi SS, Nagai Y, Watanabe K, Ma M, Veeraveedu PT, Prakash P, Kamal FA, Abe Y, Yamaguchi K, Tachikawa H, Kodama M, Aizawa Y. Chymase inhibition reduces the progression to heart failure after autoimmune myocarditis in rats. *Exp Biol Med (Maywood)* 232: 1213–1221, 2007. doi:10.3181/0703-RM-85.
- Luo Y, Zhang H, Yu J, Wei L, Li M, Xu W. Stem cell factor/mast cell/ CCL2/monocyte/macrophage axis promotes Coxsackievirus B3 myocarditis and cardiac fibrosis by increasing Ly6C<sup>high</sup> monocyte influx and fibrogenic mediators production. *Immunology* 167: 590–605, 2022. doi:10.1111/imm.13556.
- Ngkelo A, Richart A, Kirk JA, Bonna P, Vilar J, Lemitre M, Marck P, Branchereau M, Le Gall S, Renault N, Guerin C, Ranek MJ, Kervadec A, Danelli L, Gautier G, Blank U, Launay P, Camerer E, Bruneval P, Menasche P, Heymes C, Luche E, Casteilla L, Cousin B, Rodewald HR, Kass DA, Silvestre JS. Mast cells regulate myofibrillar calcium sensitization and heart function after myocardial infarction. *J Exp Med* 213: 1353–1374, 2016. doi:10.1084/jem.20160081.
- Kwon JS, Kim YS, Cho AS, Cho HH, Kim JS, Hong MH, Jeong SY, Jeong MH, Cho JG, Park JC, Kang JC, Ahn Y. The novel role of mast cells in the microenvironment of acute myocardial infarction. *J Mol Cell Cardiol* 50: 814–825, 2011. doi:10.1016/j.yjmcc.2011.01.019.
- Levick SP, McLarty JL, Murray DB, Freeman RM, Carver WE, Brower GL. Cardiac mast cells mediate left ventricular fibrosis in the hypertensive rat heart. *Hypertension* 53: 1041–1047, 2009. doi:10.1161/HYPERTENSIONAHA.108.123158.
- Selvaraj SP, Watanabe K, Ma M, Tachikawa H, Kodama M, Aizawa Y. Involvement of mast cells in the development of fibrosis in rats with postmyocarditis dilated cardiomyopathy. *Biol Pharm Bull* 28: 2128–2132, 2005. doi:10.1248/bpb.28.2128.
- Kologrivova I, Shtatolkina M, Suslova T, Ryabov V. Cells of the immune system in cardiac remodeling: main players in resolution of inflammation and repair after myocardial infarction. *Front Immunol* 12: 664457, 2021. doi:10.3389/fimmu.2021.664457.
- Patella V, Marino I, Arbustini E, Lamparter-Schummert B, Verga L, Adt M, Marone G. Stem cell factor in mast cells and increased mast cell density in idiopathic and ischemic cardiomyopathy. *Circulation* 97: 971–978, 1998. doi:10.1161/01.cir.97.10.971.
- Akgul A, Youker KA, Noon GP, Loebe M. Quantitative changes in mast cell populations after left ventricular assist device implantation. *ASAIO J* 51: 275–280, 2005. doi:10.1097/01.mat.0000150507.61120.00.
- Battle M, Perez-Villa F, Lazaro A, Garcia-Pras E, Ramirez J, Ortiz J, Orús J, Roque M, Heras M, Roig E. Correlation between mast cell density and myocardial fibrosis in congestive heart failure patients. *Transplant Proc* 39: 2347–2349, 2007. doi:10.1016/j.transproceed.2007.06.047.
- Sandstedt J, Sandstedt M, Lundqvist A, Jansson M, Sopsakis VR, Jeppsson A, Hultén LM. Human cardiac fibroblasts isolated from patients with severe heart failure are immune-competent cells mediating an inflammatory response. *Cytokine* 113: 319–325, 2019. doi:10.1016/j.cyto.2018.09.021.
- Sandstedt M, Rotter Sopsakis V, Lundqvist A, Vukusic K, Oldfors A, Dellgren G, Sandstedt J, Hultén LM. Hypoxic cardiac fibroblasts from failing human hearts decrease cardiomyocyte beating frequency in an ALOX15 dependent manner. *PLoS One* 13: e0202693, 2018. doi:10.1371/journal.pone.0202693.
- Sandstedt M, Vukusic K, Ulfenborg B, Jonsson M, Mattsson Hultén L, Dellgren G, Jeppsson A, Synergren J, Sandstedt J. Human intracardiac SSEA4<sup>+</sup> CD34<sup>+</sup> cells show features of cycling, immature cardiomyocytes and are distinct from side population and C-kit<sup>+</sup> CD45<sup>+</sup> cells. *PLoS One* 17: e0269985, 2022 [Erratum in *PLoS One* 20: e0322513, 2025]. doi:10.1371/journal.pone.0269985.
- Vukusic K, Sandstedt M, Jonsson M, Jansson M, Oldfors A, Jeppsson A, Dellgren G, Lindahl A, Sandstedt J. The atrioventricular junction: a potential niche region for progenitor cells in the adult human heart. *Stem Cells Dev* 28: 1078–1088, 2019. doi:10.1089/scd.2019.0075.
- Sandstedt M, Vukusic K, Johansson M, Jonsson M, Magnusson R, Mattsson Hultén L, Dellgren G, Jeppsson A, Lindahl A, Synergren J, Sandstedt J. Regional transcriptomic profiling reveals immune system enrichment in nonfailing atria and all chambers of the failing human heart. *Am J Physiol Heart Circ Physiol* 325: H1430–H1445, 2023. doi:10.1152/ajpheart.00438.2023.
- Sandstedt M, Jonsson M, Asp J, Dellgren G, Lindahl A, Jeppsson A, Sandstedt J. Intracellular flow cytometry may be combined with good quality and high sensitivity RT-qPCR analysis. *Cytometry A* 87: 1079–1089, 2015. doi:10.1002/cyto.a.22783.
- R Core Team. R: A Language and Environment for Statistical Computing. Vienna, Austria: R Foundation for Statistical Computing, 2020. <https://www.r-project.org/>.
- Forman MF, Brower GL, Janicki JS. Rat cardiac mast cell maturation and differentiation following acute ventricular volume overload. *Inflamm Res* 55: 408–415, 2006. doi:10.1007/s00011-006-6016-z.
- Widiapradja A, Manteufel EJ, Dehlin HM, Pena J, Goldspink PH, Sharma A, Kolb LL, Imig JD, Janicki JS, Lu B, Levick SP. Regulation of cardiac mast cell maturation and function by the neurokinin-1 receptor in the fibrotic heart. *Sci Rep* 9: 11004, 2019. doi:10.1038/s41598-019-47369-0.
- Legere SA, Haidl ID, Légaré JF, Marshall JS. Mast cells in cardiac fibrosis: new insights suggest opportunities for intervention. *Front Immunol* 10: 580, 2019. doi:10.3389/fimmu.2019.00580.
- Frangogiannis NG. Cardiac fibrosis. *Cardiovasc Res* 117: 1450–1488, 2021. doi:10.1093/cvr/cvaa324.

30. Murray DB, Gardner JD, Brower GL, Janicki JS. Endothelin-1 mediates cardiac mast cell degranulation, matrix metalloproteinase activation, and myocardial remodeling in rats. *Am J Physiol Heart Circ Physiol* 287: H2295–H2299, 2004. doi:10.1152/ajpheart.00048.2004.
31. Takai S, Jin D. Pathophysiological role of chymase-activated matrix metalloproteinase-9. *Biomedicines* 10: 2499, 2022. doi:10.3390/biomedicines10102499.
32. Gruber BL, Marchese MJ, Suzuki K, Schwartz LB, Okada Y, Nagase H, Ramamurthy NS. Synovial procollagenase activation by human mast cell tryptase dependence upon matrix metalloproteinase 3 activation. *J Clin Invest* 84: 1657–1662, 1989. doi:10.1172/JCI114344.
33. Levick SP, Gardner JD, Holland M, Hauer-Jensen M, Janicki JS, Brower GL. Protection from adverse myocardial remodeling secondary to chronic volume overload in mast cell deficient rats. *J Mol Cell Cardiol* 45: 56–61, 2008. doi:10.1016/j.yjmcc.2008.04.010.
34. Aldi S, Robador PA, Tomita K, Di Lorenzo A, Levi R. IgE receptor-mediated mast-cell renin release. *Am J Pathol* 184: 376–381, 2014. doi:10.1016/j.ajpath.2013.10.016.
35. Kunori Y, Muroga Y, Iidaka M, Mitsuhashi H, Kamimura T, Fukamizu A. Species differences in angiotensin II generation and degradation by mast cell chymases. *J Recept Signal Transduct Res* 25: 35–44, 2005. doi:10.1081/rrs-200054355.
36. Klickstein LB, Kaempfer CE, Wintroub BU. The granulocyte-angiotensin system. Angiotensin I-converting activity of cathepsin G. *J Biol Chem* 257: 15042–15046, 1982.
37. Mora-Ruiz MD, Blanco-Favela F, Chávez Rueda AK, Legorreta-Haquet MV, Chávez-Sánchez L. Role of interleukin-17 in acute myocardial infarction. *Mol Immunol* 107: 71–78, 2019. doi:10.1016/j.molimm.2019.01.008.
38. Liu Y, Lu H, Zhang C, Hu J, Xu D. Recent advances in understanding the roles of T cells in pressure overload-induced cardiac hypertrophy and remodeling. *J Mol Cell Cardiol* 129: 293–302, 2019. doi:10.1016/j.yjmcc.2019.01.005.
39. Thanikachalam PV, Ramamurthy S, Mallapu P, Varma SR, Narayanan J, Abourehab MA, Kesharwani P. Modulation of IL-33/ST2 signaling as a potential new therapeutic target for cardiovascular diseases. *Cytokine Growth Factor Rev* 71–72: 94–104, 2023. doi:10.1016/j.cytogfr.2023.06.003.
40. Lee CG, Homer RJ, Zhu Z, Lanone S, Wang X, Koteliansky V, Shipley JM, Gotwals P, Noble P, Chen Q, Senior RM, Elias JA. Interleukin-13 induces tissue fibrosis by selectively stimulating and activating transforming growth factor beta(1). *J Exp Med* 194: 809–821, 2001. doi:10.1084/jem.194.6.809.
41. Alvarez-Argote S, Paddock SJ, Flinn MA, Moreno CW, Knas MC, Almeida VA, Buday SL, Bakhshian Nik A, Patterson M, Chen YG, Lin CW, O'Meara CC. IL-13 promotes functional recovery after myocardial infarction via direct signaling to macrophages. *JCI Insight* 9: e172702, 2024. doi:10.1172/jci.insight.172702.
42. Bartekova M, Radosinska J, Jelemensky M, Dhalla NS. Role of cytokines and inflammation in heart function during health and disease. *Heart Fail Rev* 23: 733–758, 2018. doi:10.1007/s10741-018-9716-x.
43. Kulinski JM, Muñoz-Cano R, Olivera A. Sphingosine-1-phosphate and other lipid mediators generated by mast cells as critical players in allergy and mast cell function. *Eur J Pharmacol* 778: 56–67, 2016. doi:10.1016/j.ejphar.2015.02.058.
44. Taketomi Y, Murakami M. Regulatory roles of phospholipase A<sub>2</sub> enzymes and bioactive lipids in mast cell biology. *Front Immunol* 13: 923265, 2022. doi:10.3389/fimmu.2022.923265.
45. Colazzo F, Gelosa P, Tremoli E, Sironi L, Castiglioni L. Role of the cysteinyl leukotrienes in the pathogenesis and progression of cardiovascular diseases. *Mediators Inflamm* 2017: 2432958, 2017. doi:10.1155/2017/2432958.
46. Qiu H, Liu JY, Wei D, Li N, Yamoah EN, Hammock BD, Chiamvimonvat N. Cardiac-generated prostanoids mediate cardiac myocyte apoptosis after myocardial ischaemia. *Cardiovasc Res* 95: 336–345, 2012. doi:10.1093/cvr/cvs191.
47. Becher UM, Ghanem A, Tiyerili V, Fürst DO, Nickenig G, Mueller CF. Inhibition of leukotriene C4 action reduces oxidative stress and apoptosis in cardiomyocytes and impedes remodeling after myocardial injury. *J Mol Cell Cardiol* 50: 570–577, 2011. doi:10.1016/j.yjmcc.2010.11.013.
48. Hamamura K, Yoshida Y, Oyama K, Li J, Kawano S, Inoue K, Toyooka K, Yamadera M, Matsunaga N, Matsumura T, Aritake K. Hematopoietic prostaglandin d synthase is increased in mast cells and pericytes in autopsy myocardial specimens from patients with Duchenne muscular dystrophy. *Int J Mol Sci* 25: 1846, 2024. doi:10.3390/ijms25031846.
49. Berkowicz P, Kij A, Walczak M, Chlopicki S. Eicosanoid profiling in effluent of isolated perfused heart of Tgαq\*44 mice with advanced heart failure. *J Physiol Pharmacol* 70: 135–142, 2019. doi:10.26402/jpp.2019.1.13.
50. Ma K, Yang J, Shao Y, Li P, Guo H, Wu J, Zhu Y, Zhang H, Zhang X, Du J, Li Y. Therapeutic and prognostic significance of arachidonic acid in heart failure. *Circ Res* 130: 1056–1071, 2022. doi:10.1161/CIRCRESAHA.121.320548.
51. Varricchi G, Marone G, Kovanen PT. Cardiac mast cells: underappreciated immune cells in cardiovascular homeostasis and disease. *Trends Immunol* 41: 734–746, 2020. doi:10.1016/j.it.2020.06.006.